Spin-Valve-Like Magnetoresistance in Mn_2NiGa at Room Temperature

Sanjay Singh,[1] R. Rawat,[1] S. Esakki Muthu,[2] S. W. D'Souza,[1] E. Suard,[3] A. Senyshyn,[4] S. Banik,[1,5] P. Rajput,[6] S. Bhardwaj,[1] A. M. Awasthi,[1] Rajeev Ranjan,[7] S. Arumugam,[2] D. L. Schlagel,[8] T. A. Lograsso,[8] Aparna Chakrabarti,[5] and S. R. Barman[1,*]

[1]*UGC-DAE Consortium for Scientific Research, Khandwa Road, Indore 452001, India*
[2]*Centre for High Pressure Research, School of Physics, Bharathidasan University, Tiruchirappalli 620024, India*
[3]*Institut Laue-Langevin, BP 156, 38042 Grenoble Cedex 9, France*
[4]*Forschungsneutronenquelle Heinz Maier-Leibnitz FRM-II, Technische Universität München, Lichtenbergstrasse 1, 85747 Garching bei München, Germany*
[5]*Raja Ramanna Centre for Advanced Technology, Indore 452013, India*
[6]*European Synchrotron Radiation Facility, 6 rue Jules Horowitz, F-38000 Grenoble, France*
[7]*Department of Materials Engineering, Indian Institute of Science, Bangalore 560012, India*
[8]*Division of Materials Science and Engineering, Ames Laboratory, Ames, Iowa 50011, USA*

(Received 15 May 2012; published 10 December 2012)

Spin valves have revolutionized the field of magnetic recording and memory devices. Spin valves are generally realized in thin film heterostructures, where two ferromagnetic (FM) layers are separated by a nonmagnetic conducting layer. Here, we demonstrate spin-valve-like magnetoresistance at room temperature in a bulk ferrimagnetic material that exhibits a magnetic shape memory effect. The origin of this unexpected behavior in Mn_2NiGa has been investigated by neutron diffraction, magnetization, and *ab initio* theoretical calculations. The refinement of the neutron diffraction pattern shows the presence of antisite disorder where about 13% of the Ga sites are occupied by Mn atoms. On the basis of the magnetic structure obtained from neutron diffraction and theoretical calculations, we establish that these antisite defects cause the formation of FM nanoclusters with parallel alignment of Mn spin moments in a Mn_2NiGa bulk lattice that has antiparallel Mn spin moments. The direction of the Mn moments in the soft FM cluster reverses with the external magnetic field. This causes a rotation or tilt in the antiparallel Mn moments at the cluster-lattice interface resulting in the observed asymmetry in magnetoresistance.

DOI: 10.1103/PhysRevLett.109.246601 PACS numbers: 72.15.Gd, 61.05.fm, 75.50.Gg

Giant magnetoresistance and tunneling magnetoresistance effects observed in spin valves have completely transformed the technology of magnetic recording [1,2]. A spin valve has two different resistance states that can be switched by changing the direction of the applied magnetic field, resulting in asymmetric magnetoresistance (MR). Spin valves are obtained in multilayer thin films [3]. But, spin-valve-like behavior in a bulk functional material is unexpected and has not been observed before. In this Letter, we report spin-valve-like MR in a magnetic shape memory alloy (MSMA), Mn_2NiGa, and discuss its basic origin related to the intricate interplay of magnetism and disorder. MSMAs have emerged as an important class of smart material in recent years because they exhibit interesting physics [4–6] as well as properties of technological importance, such as large magnetic field induced reversible strain (MFIS) [7,8], magnetoresistance [9–11], and magnetocaloric effect [12]. Some years back, it was shown by Liu *et al.* that Mn_2NiGa exhibits about 4% field controllable MFIS at 1.8 T applied magnetic field [13]. A major advantage of Mn_2NiGa is its high magnetic ordering temperature (588 K). Powder x-ray diffraction studies showed the presence of a modulated structure in Mn_2NiGa [14], which is generally expected for a MSMA that exhibits MFIS [7]. Density functional theory showed that Mn_2NiGa is ferrimagnetic with antiparallel alignment of Mn spin moments [15,16].

Mn_2NiGa single crystal was grown in the cubic parent phase by the Bridgman method [17]. Polycrystalline ingots of Mn_2NiGa were prepared in an arc furnace under argon atmosphere by the standard method [14]. MR was measured using a superconducting magnet from Oxford Instruments, Inc., U. K. up to a maximum magnetic field of 8 T. The specimens were cooled in zero field from 300 K and the measurements were performed by varying $\mu_0 H$ (referred to as H henceforth) in the following sequence: 0 to 8 to 0 to -8 to 0 T. MR has been calculated as $\frac{\Delta\rho}{\rho_0} = \frac{(\rho_H - \rho_0)}{\rho_0}$, where ρ_H and ρ_0 are the resistivities in H and zero field, respectively. Powder neutron diffraction was performed using neutrons of wavelength 1.59 Å at room temperature (RT) at the high resolution neutron diffractometer D2B in Institut Laue-Langevin, Grenoble. The analysis of the neutron diffraction pattern was performed using the FULLPROF software package [18]. The magnetization measurements were performed by means of PPMS-9 T using a vibrating sample magnetometer module and SQUID-VSM (oven option) from Quantum Design, Inc., U.S. The electronic structure calculations have been

carried out using the fully spin-polarized relativistic Korringa-Kohn-Rostocker (SPRKKR) method including the coherent potential approximation (CPA) [19]. The calculations have been performed using the Perdew-Burke-Ernzerhof generalized gradient approximation [20] with 500 k points in the irreducible Brillouin zone. The CPA tolerance and the energy convergence criterion were set to 10^{-5} Ry. An angular momentum expansion up to $l_{\max} = 3$ for each atom type was used.

The field dependence of MR is generally symmetric about the direction of the magnetic field. Intriguingly, in Mn_2NiGa, an asymmetry in MR around $H = 0$ [Fig. 1(a)] is clearly observed with the reversal of field direction, in close resemblance with that observed for an antiferromagnetic (AFM) tunnel junction reported recently [21]. The asymmetry direction is the direction in which the field is first applied. The MR curves retrace as the field is swept from positive to negative. The asymmetric component of MR(H) defined as $[\mathrm{MR}(H) - \mathrm{MR}(-H)]/2$ shows that the asymmetry persists over an extended temperature range from 300 to 5 K [Figs. 1(a)–1(d)]. The sudden increase in MR(ΔMR) is observed within $H = \pm 50$ mT, whose quantitative estimate is about 0.03% at 300 K. This value does not, however, increase as the temperature decreases [Fig. 1(d)]. The symmetric part of MR defined as $[\mathrm{MR}(H) + \mathrm{MR}(-H)]/2$ is negative in the temperature range 300–100 K [Figs. 1(a) and 1(b)]. It varies almost linearly with field and is governed by the s-d scattering interaction [9,11]. At 50 and 5 K, although MR is positive up to 8 T, it exhibits a crossover behavior: MR increases up to about 3 T and decreases thereafter. To explain the positive MR, it may be noted that well below the magnetic transition temperature (588 K) the influence of s-d scattering on MR reduces with temperature [11]. Positive MR due to Lorentz contribution could arise if the product of cyclotron frequency and relaxation time is large. This is valid for highly ordered crystals or at very large field. But, in Mn_2NiGa, considerable disorder exists (as discussed latter), and hence this contribution is ruled out as the origin of positive MR. Rather, application of the magnetic field on antiparallel Mn spins at low temperature introduces spin fluctuations, which increase the resistivity resulting in positive MR. This has been observed earlier in a related Mn excess Ni-Mn-Ga system [10].

MR for polycrystalline Mn_2NiGa also exhibits very similar behavior [22], showing that the asymmetry is neither related to any crystallographic direction nor the grain boundaries hinder this phenomenon. This is very important from the viewpoint of practical application, since polycrystals are obviously less expensive. Furthermore, this effect is not sensitive to stoichiometry, and even non-stoichiometric compositions like $Mn_{1.7}Ni_{1.3}Ga$, (T_M = 168 K, T_C = 550 K) exhibit this effect. However, it is noteworthy that for specimens with relatively less Mn

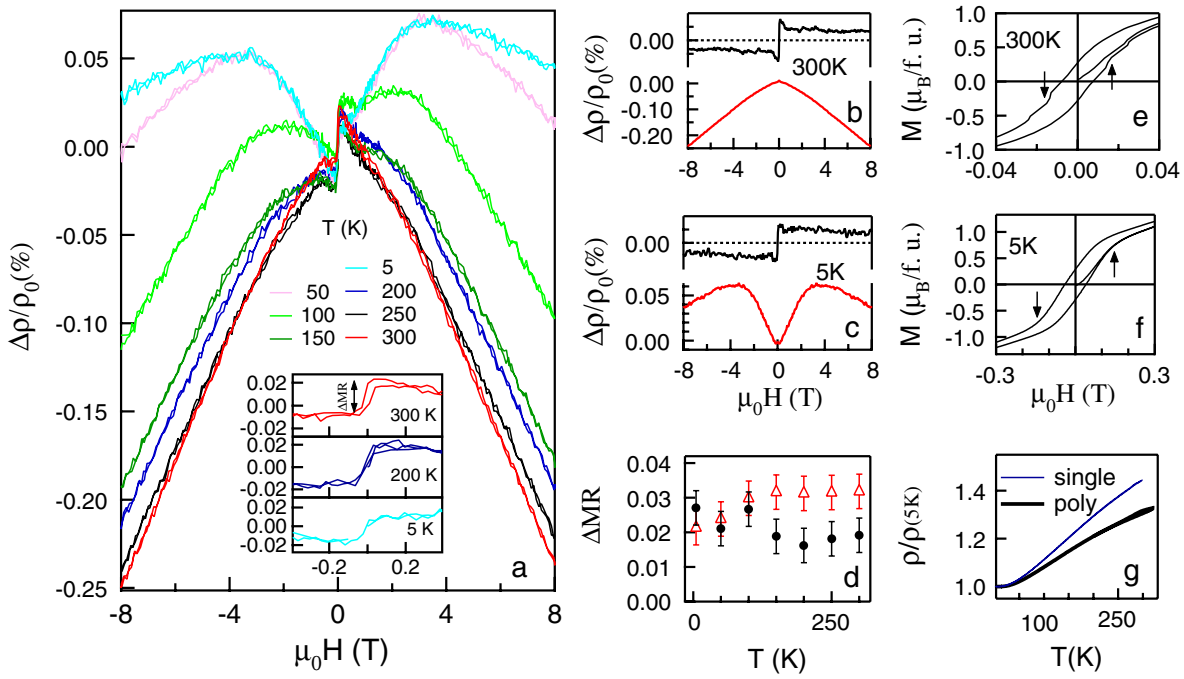

FIG. 1 (color online). (a) Magnetic field dependence of the longitudinal isothermal magnetoresistance ($\Delta\rho/\rho_0$) of Mn_2NiGa at different temperatures: 300 K (bottom curve) to 5 K (top curve). The magnetoresistance data at 300, 200, and 5 K are shown in an expanded scale in the inset; ΔMR is indicated. The asymmetric and symmetric components of MR at (b) 300 K and (c) 5 K. (d) ΔMR for single crystalline (open red triangle) and polycrystalline (filled black circle) Mn_2NiGa as a function of temperature. $M(H)$ hysteresis loops at (e) 300 K and (f) 5 K; the steps or the change in slope are shown by arrows. (g) Comparison of the single and polycrystal resistivities as a function of temperature in zero field.

content, for example, $Mn_{1.25}Ni_{1.75}Ga$ ($T_M = 76$ K, $T_C = 380$ K), Ni_2MnGa, and Ni excess Ni_2MnGa, the asymmetry in MR is not observed [9,10]. This indicates that this behavior might be typical of compositions close to Mn_2NiGa. To investigate the origin of asymmetric MR in Mn_2NiGa, we have studied its magnetic and transport properties [Figs. 1(e)–1(g)].

The saturation magnetization of Mn_2NiGa at 5 K is about $1.5\mu_B$/formula unit (f.u.) [22], in agreement with earlier studies [13,23]. The hysteresis loops are narrow with a coercive field of about 8 and 38 mT at 300 and 5 K, respectively [Figs. 1(e) and 1(f)]. Generally, the presence of disorder in a metal is reflected by its residual resistivity ratio (RRR), i.e., the ratio of the resistivities at 300 and 5 K. RRR has been used to correlate the influence of antisite disorder on the magnetic properties of Ni-Mn-Ga where it is found to decrease with increasing antisite disorder [24]. For Mn_2NiGa, RRR for the single crystal (1.4) is marginally higher than the polycrystal (1.3), which indicates that these have comparable antisite disorder [Fig. 1(g)]. Note that ΔMR is also similar between the single and the polycrystal [Fig. 1(d)]. So, the nature of the disorder might be crucial to understand the intriguing MR behavior, and we have investigated this by powder neutron diffraction, as discussed below.

The crystal structure refinement of Mn_2NiGa based on our powder neutron diffraction data could be performed with a tetragonal unit cell. The space group turns out to be $I4/mmm$ with the following initial atomic positions: Ni and Mn_{Ni} at $4d$ (0, 0.5, 0.25), Mn_{Mn} at $2a$ (0, 0, 0) and Ga at $2b$ (0, 0, 0.5). Note that Mn_X refers to a Mn atom at the X(X = Ni, Mn, Ga) atom site of Ni_2MnGa where Ni, Mn, and Ga atoms occupy $4d$, $2a$, and $2b$ sites, respectively [Fig. 2(e)]. In our previous work [14], we have shown that the stress present due to grinding the sample into powder stabilizes the tetragonal structure (i.e., the martensite phase) at 300 K even though it is above M_s(= 272 K) [22,23]. However, a minuscule amount of the cubic phase is present, as observed earlier from diffraction studies [14,25].

To identify the site occupancies and disorder, the diffraction pattern above $2\theta = 60°$ has been fitted. This is because the magnetic contribution in the peak intensities are very small in this 2θ range. The sizable difference in the nuclear scattering amplitude for Ni, Mn, and Ga (10.3, −3.73, and 7.29 fm, respectively) allows the determination of the actual atomic occupancies and the degree of disorder

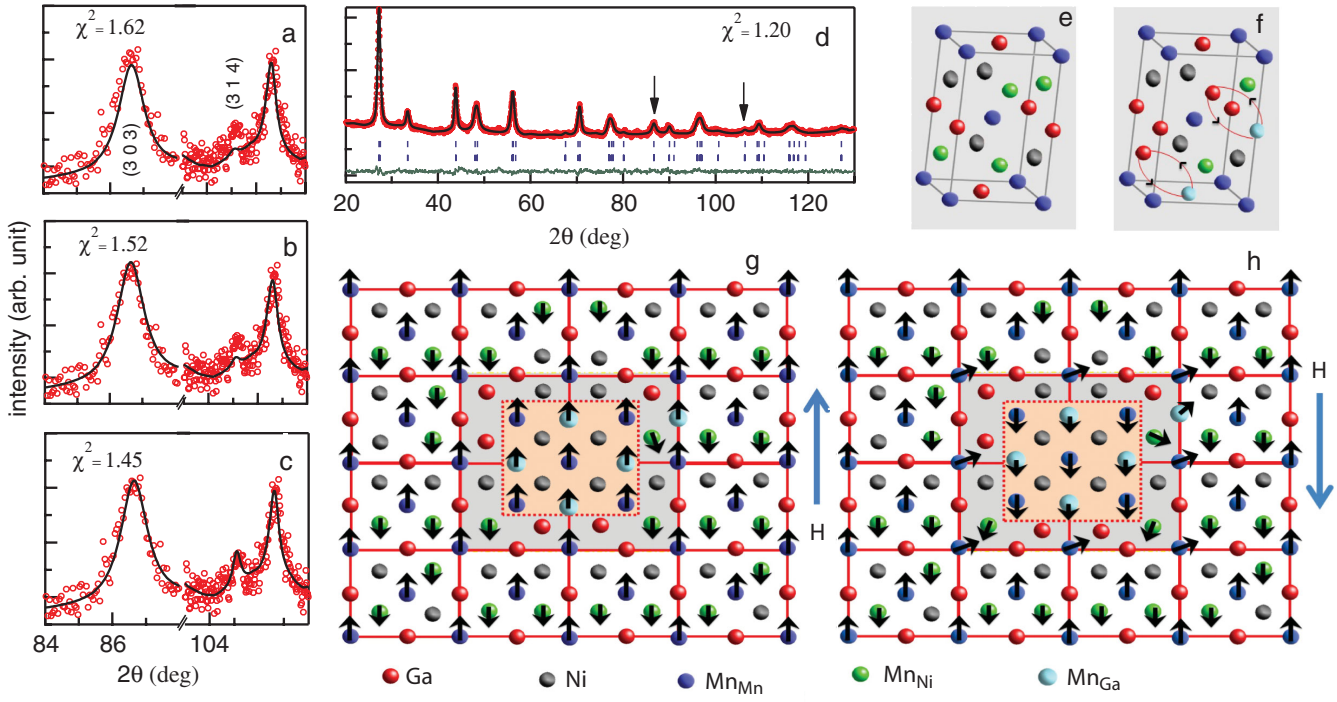

FIG. 2 (color). Powder neutron diffraction studies on Mn_2NiGa where the (3 0 3) and (3 1 4) Bragg peaks at RT (red circles) have been fitted (black solid lines) considering (a) no disorder, (b) Mn_{Mn}-Ga disorder, and (c) Mn_{Ni}-Ga disorder. (d) The observed (red circle) and calculated (black solid line) neutron diffraction pattern for Mn_2NiGa at 300 K. The vertical arrows indicate (3 0 3) and (3 1 4) Bragg peaks. The green curve shows the difference between observed and calculated patterns. The upper vertical ticks are nuclear Bragg peak positions; the lower vertical ticks are the magnetic Bragg positions. (e) The tetragonal unit cell of Mn_2NiGa. (f) The tetragonal unit cell showing the Mn_{Ni}-Ga antisite defects. (g),(h) Schematic diagrams of the ab plane of Mn_2NiGa showing the tilt or rotation of the localized spins at the interface (light gray region) of the ferromagnetic nanocluster (light orange square, formed by four Mn_{Ni}-Ga antisite defects) and the AFM lattice as the external magnetic field (H) is reversed within ± 50 mT. The arrows represent the spin moment direction, whereas their length is proportional to the magnitude.

in Mn_2NiGa. Figures 2(a)–2(c) show a comparison of the fitting for (3 0 3) and (3 1 4) Bragg peaks for the different atomic structures. A fit without considering antisite disorder was unsatisfactory [$\chi^2 = 1.62$, Fig. 2(a)]. Consideration of antisite disorder between Ni-Mn_{Mn} and Ni-Ga did not improve the fitting, while the fit improved to some extent when antisite disorder between Mn_{Mn} and Ga was considered [$\chi^2 = 1.52$, Fig. 2(b)]. However, when antisite disorder between Mn_{Ni} and Ga is considered, the best fit with lowest $\chi^2 = 1.45$ was obtained [Fig. 2(c)]. The Mn_{Ni}-Ga antisite defects are shown in Fig. 2(f). The refined site occupancies in Table I exhibit Mn_{Ni}-Ga antisite disorder with about 13% of the Ga sites being occupied by the Mn atoms. The Ga atoms displaced from the 2*b* site occupy the 4*d* site.

The refinement for the full range considering both the structural and the magnetic part is shown in Fig. 2(d). The refined moments at 4*d*, 2*a*, and 2*b* sites are -0.38, 1.32, and $0.3\mu_B$, respectively (Table I). The negative moment at the 4*d* site indicates that Mn_{Ni} and Mn_{Mn} spins are antiparallel, which is in agreement with density functional theory [15,16]. The moment of $0.3\mu_B$ at the 2*b* site (Table I) arises primarily from Mn_{Ga}, since Ga does not have magnetic moment. Interestingly, both 2*a* and 2*b* site moments are positive, indicating that Mn_{Mn} and Mn_{Ga} spins are in parallel orientation. However, it was observed that the 2*b* site moment is correlated with the isotropic displacement parameter resulting in a large uncertainty of the moment values. A large error of 60% for the 4*d* site with a $0.05\mu_B$ moment was reported earlier; the difference of the moment values with our result is possibly because antisite disorder was not considered in Ref. [25].

In order to theoretically estimate the magnetic moments in Mn_2NiGa including the Mn_{Ni}-Ga antisite disorder obtained from neutron diffraction, we have performed the SPRKKR calculations in the multiple scattering theory formalism within CPA [19]. In the calculation, the crystal structure as given in Table I has been used. For example, the occupancies considered at the sites 2*b* and 4*d* are $Ga_{0.88} + Mn_{0.12}$ and $Ni_{0.5} + Mn_{0.44} + Ga_{0.06}$, respectively.

TABLE I. Parameters obtained from the refinement of the neutron diffraction pattern of Mn_2NiGa at 300 K. The value of the profile factor (R_p) and the weighted profile factor (R_{wp}) are 23 and 16.2, respectively.

Space group	$I4/mmm$		
Lattice parameters	$a = b = 3.915$ Å,	$c = 6.712$ Å	
Atomic site	4*d*	2*a*	2*b*
Ni occupancy	0.5	0	0
Mn occupancy	0.439(4) [Mn_{Ni}]	1 [Mn_{Mn}]	0.123(7) [Mn_{Ga}]
Ga occupancy	0.061(4)	0	0.877(7)
Site moment (μ_B)	−0.38(6)	1.32(7)	0.3(8)
B_{iso}(Å^2)	2.70(07)	1.71(06)	1.81(06)

In complicated magnetic systems, the self-consistency calculations might converge to a local minimum [16,26]. So, to obtain the lowest energy magnetic state, different starting configurations of parallel and antiparallel collinear moments of Mn_{Ni}, Mn_{Mn}, and Mn_{Ga} have been considered. We find that in the ground state Mn_{Ga} is parallel to the Mn_{Mn} spin moment, whereas Mn_{Ga} is antiparallel to Mn_{Ni}. Thus, theory supports the results obtained from neutron diffraction and indicates the existence of ferromagnetic (FM) clusters. The local spin (orbital) moments for Ni, Mn_{Ni}, Mn_{Mn}, and Mn_{Ga} are 0.40 (0.035), −2.39 (− 0.024), 3.34 (0.022), and 3.41 (0.014)μ_B, respectively. The AFM interaction between Mn_{Ni} and Mn_{Mn}, which are nearest neighbors 2.578 Å apart, results from the exchange pair interaction at relatively short Mn-Mn distance [27]. On the other hand, Mn_{Ga} is the next nearest neighbor of Mn_{Mn} at a separation of 2.769 Å, and their interaction is ferromagnetic [28].

The results of the refinement of the neutron diffraction data supported by theoretical calculations demonstrate the presence of FM clusters [shown schematically in Figs. 2(g) and 2(h) as light orange squares] due to Mn_{Ga}-Mn_{Mn} FM coupling originating from the antisite disorder. Since these defects are randomly distributed, an estimate of the cluster size is of the order of the unit cell, i.e., 6–7 Å (< 1 nm). Interestingly, evidence of a soft FM phase is observed as steps in the magnetization curve [shown by arrows in Figs. 1(e) and 1(f)]. An estimate of the FM cluster moment from the size of the step is about $3\mu_B$ at 300 K, assuming that one antisite defect constitutes the cluster and the result from neutron diffraction that 13% of the Ga sites are occupied by the Mn atoms. From our theoretical calculations, the cluster moment could be considered to be the moment in a unit cell with one Ga-Mn antisite defect. This turns out to be $4.25\mu_B$/f.u. at zero temperature. Therefore, there is a reasonable agreement between the theoretical and experimental estimates.

The shift in the hysteresis loop that is generally observed in exchange bias systems has not been observed by us at RT in Mn_2NiGa polycrystal within our measurement accuracy after 5 T field cooling from 650 K. The absence of exchange bias is possibly related to the nanosize of the FM clusters. This argument is supported by the result that in 3 nm FM Co clusters with AFM CoO shell, exchange bias was not observed below a critical size because the anisotropic energy of the AFM shell is smaller than the interface exchange energy [29]. However, in spite of the FM clusters being small, being a transport property, MR is influenced sensitively by electron scattering. Initially, when a magnetic field is applied, the FM cluster moment and the net moment of the ferrimagnetic matrix are oriented parallel to the field direction. The moments at the interface are locked accordingly. When the magnetic field direction is changed, the moments at the interface will encounter a rotated or tilted frustrated state due to antiparallel alignment of the

cluster and the matrix. A simplified version of this scenario is shown in Figs. 2(g) and 2(h) for low field. Here, these two arrangements can result in different resistivities. Under free-electron approximation, the mean free path is estimated to be ≈ 2 Å, as the resistivity is $\approx 200\ \mu\Omega$ cm at 5 K. This is less than the average intercluster separation (> 20 Å) and suggests that interface scattering could be the origin of this effect. Since in the present case, ΔMR remains unchanged with varying temperature, it can be inferred that the mean free path variation (RRR 1.3–1.4) does not have significant effect on it.

In conclusion, a spin-valve-like effect in MR at room temperature originating from antisite disorder is demonstrated in Mn_2NiGa. This effect persists over a wide temperature range 5–300 K and is observed for both polycrystal and single crystal specimens. Evidence of about 13% Mn_{Ni}-Ga antisite disorder and the magnetic structure obtained from neutron diffraction supported by SPRKKR calculations and magnetization measurements establish the presence of soft ferromagnetic nanoclusters. These FM clusters that occur in the ferrimagnetic lattice due to antisite disorder are responsible for the spin-valve-like behavior of magnetoresistance in bulk Mn_2NiGa. Further studies on controlled growth of FM nanoclusters in a bulk lattice may enhance ΔMR and also shed more light on the understanding of this effect.

J. Rodríguez-Carvajal, T. Roisnel, C. Ritter, A. Daoud-Aladine, M. Avdeev, H. Ebert, and M. Offenberger are thanked for useful discussions and support. R. J. Choudhary is thanked for providing the field cooled magnetization data from 650 K. S. S. and S. W. D. thank CSIR for support. Funding from the Max Planck Partner Group project, Department of Science and Technology, Government of India, and Institut Laue-Langevin, France, is gratefully acknowledged. D. L. S. and T. A. L. acknowledge the support of the U.S. Department of Energy, Materials Science and Engineering Division.

*barmansr@gmail.com

[1] C. Chappert, A. Fert, and F. N. V. Dau, Nature Mater. **6**, 813 (2007).
[2] S. A. Wolf, D. D. Awschalom, R. A. Buhrman, J. M. Daughton, S. von Molnár, M. L. Roukes, A. Y. Chtchelkanova, and D. M. Treger, Science **294**, 1488 (2001).
[3] B. Dieny, V. S. Speriosu, S. S. P. Parkin, B. A. Gurney, D. R. Wilhoit, and D. Mauri, Phys. Rev. B **43**, 1297 (1991).
[4] T. Krenke, E. Duman, M. Acet, E. F. Wassermann, X. Moya, L. Mañosa, and A. Planes, Nature Mater. **4**, 450 (2005).
[5] I. Takeuchi *et al.*, Nature Mater. **2**, 180 (2003).
[6] L. Mañosa, D. González-Alonso, A. Planes, E. Bonnot, M. Barrio, J.-L. Tamarit, S. Aksoy, and M. Acet, Nature Mater. **9**, 478 (2010).
[7] A. Sozinov, A. A. Likhachev, N. Lanska, and K. Ullakko, Appl. Phys. Lett. **80**, 1746 (2002).
[8] R. Kainuma *et al.*, Nature (London) **439**, 957 (2006).
[9] C. Biswas, R. Rawat, and S. R. Barman, Appl. Phys. Lett. **86**, 202508 (2005).
[10] S. Banik, R. Rawat, P. K. Mukhopadhyay, B. L. Ahuja, A. Chakrabarti, P. L. Paulose, S. Singh, A. K. Singh, D. Pandey, and S. R. Barman, Phys. Rev. B **77**, 224417 (2008).
[11] S. Banik, S. Singh, R. Rawat, P. K. Mukhopadhyay, B. L. Ahuja, A. M. Awasthi, S. R. Barman, and E. V. Sampathkumaran, J. Appl. Phys. **106**, 103919 (2009).
[12] F. X. Hu, B. G. Shen, J. R. Sun, and G. H. Wu, Phys. Rev. B **64**, 132412 (2001).
[13] G. D. Liu, J. L. Chen, Z. H. Liu, X. F. Dai, G. H. Wu, B. Zhang, and X. X. Zhang, Appl. Phys. Lett. **87**, 262504 (2005).
[14] S. Singh, M. Maniraj, S. W. D'Souza, R. Ranjan, and S. R. Barman, Appl. Phys. Lett. **96**, 081904 (2010).
[15] S. R. Barman, S. Banik, A. K. Shukla, C. Kamal, and A. Chakrabarti, Europhys. Lett. **80**, 57002 (2007).
[16] S. R. Barman and A. Chakrabarti, Phys. Rev. B **77**, 176401 (2008).
[17] D. L. Schlagel, Y. L. Wu, W. Zhang, and T. A. Lograsso, J. Alloys Compd. **312**, 77 (2000).
[18] J. Rodríguez-Carvajal, Physica (Amsterdam) **192B**, 55 (1993).
[19] H. Ebert *et al.*, the Munich SPRKKR package, version 5.4, http://olymp.cup.uni-muenchen.de/ak/ebert/SPRKKR.
[20] J. P. Perdew, K. Burke, and M. Ernzerhof, Phys. Rev. Lett. **77**, 3865 (1996).
[21] B. G. Park *et al.*, Nature Mater. **10**, 347 (2011).
[22] See Supplemental Material at http://link.aps.org/supplemental/10.1103/PhysRevLett.109.246601 for magnetic field dependence of isothermal magnetoresistance (Fig. S1), martensite transition temperatures and latent heat from the differential scanning calorimetry, and saturation magnetization from $M(H)$ hysteresis data (Fig. S2) of polycrystalline Mn_2NiGa.
[23] B. L. Ahuja, G. Ahmed, S. Banik, M. Itou, Y. Sakurai, and S. Barman, Phys. Rev. B **79**, 214403 (2009).
[24] S. Singh, R. Rawat, and S. R. Barman, Appl. Phys. Lett. **99**, 021902 (2011).
[25] P. J. Brown, T. Kanomata, K. Neumann, K. U. Neumann, B. Ouladdiaf, A. Sheikh, and K. R. A. Ziebeck, J. Phys. Condens. Matter **22**, 506001 (2010).
[26] A. Chakrabarti and S. R. Barman, Appl. Phys. Lett. **94**, 161908 (2009).
[27] D. Hobbs, J. Hafner, and D. Spisak, Phys. Rev. B **68**, 014407 (2003).
[28] P. Lázpita, J. M. Barandiarán, J. Gutiérrez, J. Feuchtwanger, V. A. Chernenko, and M. L. Richard, New J. Phys. **13**, 033039 (2011).
[29] A. N. Dobrynin *et al.*, Appl. Phys. Lett. **87**, 012501 (2005).